Matched-filter based algorithm for sub- to multi-cellular classification of myocyte tubule-system

Dylan F Colli[1], S Ryan Blood[1], Aparna C Sankarankutty[2], Frank B Sachse[2], Michael Frisk[3], William E Louch[3], and Peter Kekenes-Huskey[1]

[1]Department of Chemistry, University of Kentucky, Lexington, KY, USA 40506; [2]Nora Eccles Harrison Cardiovascular Research and Training Institute & Department of Bioengineering, University of Utah, Salt Lake City, UT 84112; [3]University of Oslo, Oslo, Norway

Submitted July 17, 2018

In healthy tissue of various mammals, transverse tubules (TTs) are found in a strongly conserved, striated pattern that aligns with the sarcomere network at the z-lines. In a variety of etiologies, this network is perturbed, which is believed to correlate with ineffective, dyssynchronous Ca^{2+} release and subsequent contraction. Confocal microscopy has become the de facto standard for characterization of TT networks, for which several algorithms for detecting and classifying these subcellular structures have emerged. However, to our knowledge, such algorithms are irrespective of subcellular variations in TT angle and are restricted in application to single isolated myocytes. Here we present a matched filter-based algorithm to characterize TT structure at a subcellular-level, in single cardiomyocytes through millimeter-scale tissue preparations. The algorithm utilizes 'filters' representative of intact TT structure, longitudinal remodeling, and TT absence. Application of the algorithm to cardiomyocytes isolated from SHAM, myocardial infarction (MI), and thoracic aortic banding (TAB) animal models confirm and quantify locally-heterogeneous TT structure and structural remodeling. We find significant ($p < 0.05$) increases in longitudinal remodeling within myocytes intermediate and proximal to an infarct (10 ± 2% and 12 ± 3% compared to 4 ± 2% in SHAM) as well as decreases in tubule striations within 5° of myocyte minor axis for TAB (36 ± 9%), intermediate (37 ± 4%), and proximal (34 ± 4%) MI myocytes compared to SHAM myocytes (57 ± 12%). Given the reliance of the matched filter approach on images representative of subcellular features, we anticipate the algorithm is generalizable to wide-ranging imaging applications.

INTRODUCTION

In ventricular myocytes, Ca^{2+}-induced-Ca^{2+}-release (CICR) begins with the propagation of a depolarizing action potential (AP) down the membrane, controlling sarcolemma (SL) Ca^{2+} flux from L-type calcium channel (LCC) localized primarily to SL invaginations, called transverse tubules (transverse tubule (TT)s).[1] Localized Ca^{2+} entry via LCCs trigger neighboring ryanodine receptors (RyRs) located on the sarcoplasmic reticulum (SR) membrane to open and release Ca^{2+} from SR stores.[1–4] Thus, the spatiotemporal synchrony and homogeneity of sarcolemma-bound LCC Ca^{2+} release is critical in maintaining efficacious contraction of the heart. In intact, fully-functional rat ventricular cardiomyocytes, a rete termed the transverse-axial tubule system (TATS) consisting of transverse tubules coinciding with the Z-lines of sarcomeres and axial tubules is observed.[5,6] In failing hearts, severe morphological changes in the tubule structure of cardiac ventricular myocytes correlate with impairments of critical excitation-contraction coupling (ECC) Ca^{2+} handling mechanisms[1,7] that drive Ca^{2+} dysregulation and cardiac dysfunction.[8–10]

The explosive growth in fluorescence based microscopy offers outstanding potential to probe mechanisms governing TT remodeling. However, the nature of TT remodeling can be quite diverse, with some etiologies almost strictly presenting tubule absence (see TAB in Fig. S2B), while others can actually exhibit regrowth of TTs in non-transverse arrangements (see MI in Fig. 3). Among the disease models that manifest evident changes in TT structure, distinctive patterns have emerged, from reduced TT density in type-II diabetic mice,[11] to increased density of *longitudinal* tubules with differing patterns for congenital heart failure,[12] spontaneous hypertension/heart failure (SHF),[13] and other disorders.[14] Substantial amounts of sub-micron resolution confocal microscopy data exist for several models of heart failure (HF) (concentric hypertrophy and dilated hypertrophy, for instance) in species including mice,[9,12,15–17] rabbit,[18–20] canine,[21,22] and human,[23,24] however, quantitative assessments of subcellular TT structure have been limited.

Characterization of imaging data and correlating structural features with cardiac function[25] represent significant challenges that permit computational solutions. Several algorithms have been introduced to automate the characterization of whole myocyte ultrastructure. Among these approaches is the 'TT index' or 'TT power', whereby the relative spacing and angle of TT arrangements are estimated by analysis of Fourier transformed images.,[26,27] The TT index correlates well with the severity of remodeling, but provides limited structural classification beyond orientation. More recent methods apply some level of preprocessing in order to essentially increase the amplitude of the signal arising from the TTs.[26,27] The most common metric appears to be binary thresholding, which increases contrast by converting all pixels to binary values, depending on their value relative

to a user-determined threshold. Others utilize morphological transformations which produce 'skeletonized' representations of the TT network, which tend to enhance the TT index response.[26–28] Recent uses of techniques such as histogram equalization[29] have been tuned to improve existing analysis approaches.[26–28]The advantage of these approaches is that they assume little prior knowledge about the structure of the TT network, yet their applications have been limited to single myocyte preparations.

Here we present a matched-filter based image processing algorithm for the subcellular characterization of TT structure. The method relies on user-provided images, or filters, representing features of interest, such as native TTs, longitudinal tubules, and low signal intensity regions indicating tubule absence. In contrast to methods that threshold imaging data to highlight features, this algorithm preserves a dynamic range of the original image. We outline the corresponding workflow in Fig. 1, which we use to characterize the total cellular content of intact TT structure (WT), longitudinal regrowth (LT), and tubule absence (TA) in isolated cells and whole tissue from SHAM, MI, and TAB animal models. Our results suggest that the matched filtering approach performs favorably for detecting different extents and modalities for TT configurations in confocal-microscopy-derived data, and reveal patterns of TT structure and remodeling unique to SHAM, MI and TAB cardiomyocytes. We find that the approach is robust to regional variation in subcellular structure and noise, while providing a first-of-its-kind method scalable to tissue-level imaging. Our workflow therefore provides a TT characterization strategy complementary to approaches including autoTT,[27] while its reliance on user-provided 'kernels' permit its generalization to arbitrary microscopy imaging data.

MATERIALS AND METHODS

Matched filter theory and application Matched filtering describes a procedure for detecting a known signal, s, in statistically uncorrelated noise, n, via the relationship

$$y = \hat{s}\mathbf{C_n}^{-1}\hat{m} \tag{1}$$

where m is the measured signal ($m = s + n$),[30] $\mathbf{C_n}$ is the noise covariance ($\mathbf{C_n} = \mathbb{E}[nn^T]$, where $\mathbb{E}[nn^T]$ signifies the expectation of a random, spatially distributed noise vector, n). The overarching principle in matched filtering is to identify a matched filter, $\hat{h}$, that maximizes the signal-to-noise ratio (SNR) for a measurement, $\hat{m}$,[30]

$$y = \hat{h}^T\hat{m} = \hat{h}^T\hat{s} + \hat{h}^T\hat{n}, \tag{2}$$

where $\hat{h}^T$ denotes the filter's transpose. We utilize this approach in the first stage of our workflow in order to assess the likelihood that a filter representing a feature of interest is present in a given data set. Often the signal, or multiple instances thereof, is embedded within a larger data set ($\hat{r}$), such as an image. In which case, determining the location of $\hat{s}$ within $\hat{r}$ is commonly performed by convolving the filter $\hat{h}$ with the image, $\hat{r}$

$$Y = \hat{h} * \hat{r} \tag{3}$$

$$= \mathscr{F}_N^{-1}\left[\mathscr{F}_N[\hat{h}] \cdot \mathscr{F}_N[\hat{r}]\right], \tag{4}$$

where the second line represents using discrete Fourier transforms to solve Eq. 3 via the convolution theorem. Probable detections of the filter $\hat{h}_i$ within Y are then based on identifying positions, at which the area-integrated response is above a user-specified threshold criterion, λ_i,

$$\bar{y}(\Omega) \equiv \int_\Omega y \, d\Omega > \lambda_i \tag{5}$$

where y is obtained from Eq. 2 (or via convolution) and Ω represents the area over which the signal is expected to generate a significant response. Since the images are resized to a common length scale in our approach, the area over which we chose to integrate over is arbitrary. Due to this, we chose an area with side length of a single striation for Ω. To classify where cellular ultrastructure resembles known filters, we evaluate

$$\bar{y}_i = \hat{h}_i^T m, \quad \forall h_i \in \{\hat{h}_1, \hat{h}_2, ...\}$$

The optimal filter is chosen as $\max(\{y_1, y_2, ...\})$, so long as there exists at least one y_i for which $y_i > \epsilon_i$.

Matched filter determination

Here we determine the matched filters based on manually identifying representative TT regions in the confocal data. The three morphological characteristics that we wished to identify were wild-type (WT), longitudinal tubule (LT), and TA regions. The filters are shown in Fig. S7 and are described as follows. The WT filter consisted of two separated binary TT structural elements. The complement to this filter was utilized as a penalty filter as described in Sect. S.1.4. The LT filter consisted of a one sarcomere wide longitudinal structural element with

varying intensity according to a normal distribution along the x axis. This varying intensity allowed for the emphasis of the uniquely longitudinal portion of the LT filter relative to the portion of the LT filter similarly represented in the WT filter. The TA filter was a single striation length square smoothing filter. The presence of sub-threshold pixels in the resulting smoothed image indicated the presence of sarcomere sized regions of low signal density. Details for selecting optimal threshold parameters and corresponding receiver operator characteristic (ROC) curves are provided in Sect. S.3.2.

All aforementioned numerical procedures were conducted using the PYTHON2.7 libraries NUMPY, SCIPY and OPENCV-PYTHON. Data processing was performed using scipy and jupyter notebooks. All source code will be provided at https://bitbucket.org/pkhlab/matchedmyo (currently private) ; a limited set of tests can be performed with the code here http://athena.as.uky.edu/node/6.

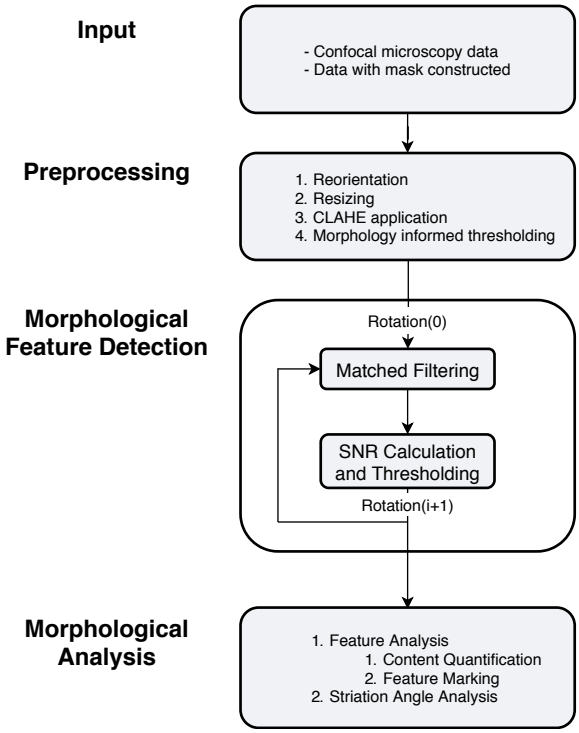

Figure 1: Unicellular matched filtering protocol consisting of 1) Input of confocal microscopy data and user generated mask for that data. 2) Integrated preprocessing routines. 3) Morphological feature detection via matched filtering and signal-to-noise ratio calculation. 4) Morphological analysis of features, feature density, and feature rotation. A detailed version of this workflow with representative images is provided in Fig. S8

RESULTS AND DISCUSSION

Model application to isolated myocytes

Rat wild-type

We first demonstrate the matched filtering approach using SHAM data in Fig. 2A), for which the intact cardiomyocytes present a highly-regular, striated pattern of TTs (see Sect. S.2.1 for details on cell isolation and imaging). It is evident from the unprocessed data in Fig. 2 that the WT cardiomyocyte exhibits a strongly conserved, striated TT pattern. Nevertheless, subregions of the cardiomyocyte present an appreciable degree of spatial and angular variation. In Fig. 2b), we present the classification results, for which the WT, TA, and LT responses are overlaid as blue, red, and green, respectively. In order to improve the classification results, we utilized a mask to obscure the cell membrane and other artifacts in the field of view. In this image, the WT response predominates over the LT and TA signals (see Fig. 2B), which we summarize in Table S3. This difference in response is a direct result of the optimization procedure outlined in Sect. S.3.2.

In principle, similar conclusions could be drawn by visual inspection of these data or application of more simplistic analyses, such as the TT power index. However, one benefit of the matched-filtering approach is the ability to detect spatially heterogeneous variations in the TT structure. For instance, the TT striations are not strictly vertical throughout the myocyte interior. Rather, the striations appear to accommodate roughly perpendicular orientations relative to the plasma membrane along the longitudinal axis. In traditional TT index or power methods, these spatial variations in angular frequencies would present a diffuse signal response in the Fourier domain, leading to a potential misclassification of subcellular structure. Because our method relies on

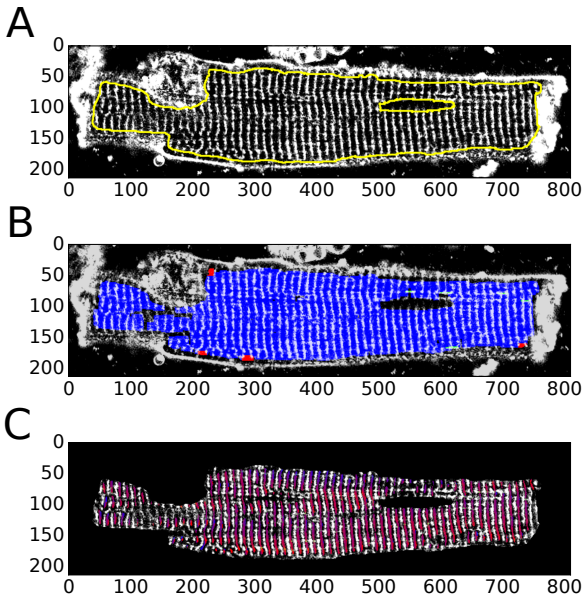

Figure 2: Algorithm application to isolated SHAM cells. Cardiomyocyte A) raw image with region of interest indicated by yellow line and B) image with transverse tubules (TT, blue), TT absence (red) and longitudinal regrowth (green) marked. C) indicates angle of TT relative to Y axis. Angle is denoted via a heatmap where pure red corresponds to a hit at the leftmost rotation angle of -25° and pure blue corresponds to a hit at the rightmost rotation angle of $+25^\circ$.

convolution, it is straightforward to quantify the variation, as we report in Table S3. Here, we find that for the myocytes considered herein, SHAM cells present $57 \pm 12\%$ of striations within 5° of the myocyte minor axis while there are significant deviations ($p < 0.05$) in the considered TAB myocytes (36 ± 9 %), intermediate MI myocytes (37 ± 4 %), and proximal MI myocytes (34 ± 4 %). We also report in Fig. 2B) significantly fewer responses from the LT filter, based on five cells. The LT responses tend to localize toward the outer sarcolemma and coincide with compact regions of high intensity signal in the raw data. We believe that these localized regions are due to folding of the sarcolemma and are therefore false positives for the LT criterion. We also note that in murine species, the TT network presents considerable branching that manifests in significant axial contributions[5] ; these features were not evident in the cells considered here owing most likely to the resolution of the microscopy data. For the TA criterion, aside from a region corresponding to the nucleus where no TT are expected, we report no significant responses.

Myocytes proximal to an infarction site

In contrast to TAB, MI can introduce a localized necrotic region in tissue. Cells adjacent to this necrotic region and border zone exhibit varying degrees of remodeling[31] Here we applied the algorithm to cardiomyocytes isolated from regions proximal (P), intermediate (I), and distal (D) to an MI. These cells were obtained from an infarcted heart after explantation, for which the border zone was removed, and the remaining non-infarcted regions of the heart were divided into 3 equal-sized regions (proximal, intermediate, and distal) as described in.[32] We find that proximal tissue exhibits substantial increase in longitudinal tubule growth, as well as a decrease in TT-density, the latter of which was observed with decreased severity compared to the congestive heart failure (CHF) tissue (see Fig. 3 and Table S3). Myocytes from the intermediate region presented both tubule absence and evidence of longitudinal regrowth, although to a lesser extent than the proximal cells (see Fig. S5 for cells considered in this study). Finally, we confirm for distally-derived tissue that for the four metrics used in this study, WT, LT, TA, and striation angle, the differences observed were insignificant compared to SHAM myocytes. The main implication of this finding is that the MI etiology appears to give rise to regrowth and TT reorganization that is distinct from tubule absence patterns exhibited in CHF. Further, the extent of regrowth parallels distance from MI while TT density appears to have an inverse relationship with proximity to the MI.

Infarcted cardiac tissue

In the preceding section, we applied our algorithm to isolated cardiomyocytes. A disadvantage of restricting analyses to isolated cells is that there is limited information about their local tissue environment, such as the precise orientation of cells relative to an MI. Whereas evaluation of the isolated myocytes we considered up to this point can be carried out with ease on standard computing resources, tissue-level characterization presents unique challenges, including segmenting out non-cardiac regions as well as the overall computational burden of processing much larger datasets. Given the large sizes of these images, we utilized a graphics processing unit (gpu)-acceleration to evaluate the Fast Fourier Transform (FFT)s utilized in our matched filtering approach (see

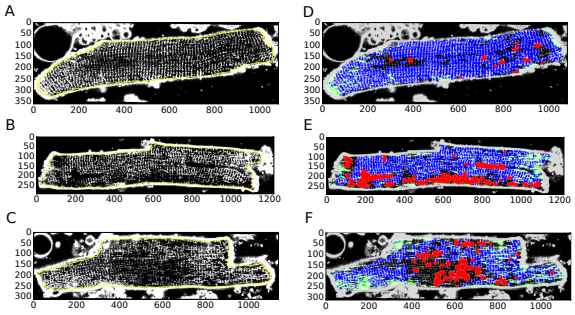

Figure 3: Algorithm application to cells isolated from infarcted myocardium. Raw (left) and annotated (right) tissue from cells A) distal, B) intermediate and C) proximal to a myocardial infarction zone. Raw images have regions of interest contained within yellow lines.

Sect. S.2.5 for more details). For the first challenge, an advantage of the matched filter approach is that it is generally insensitive to image features that bear little resemblance to the convolved filter, such as the linear striations of the TT network relative to the sinuous edges of cardiomyocytes in intact tissue. Thus, for these analyses, we do not mask the cell boundaries as done for the isolated myocytes. In Fig. 4 we analyze subsections of a 3.9x4.1 mm^2 tissue sample from a rabbit infarct model using the WT filter. We demonstrate responses are almost exclusively within the cardiomyocyte interiors with little overlap with membrane comprising the interface shared by adjacent cells. However, unlike the isolated myocyte for which the TTs are more uniformly labeled throughout the cell interior, many of the cells in the tissue appear to be incompletely labeled. As such, our data indicates a smaller percentage of TT content relative to isolated cardiomyocytes. Here, we show the relative propensity for the TT features are most prominent in regions distal to the MI. Fig. 4A and C represent tissue distal to an infarct where Fig. 4B and D represent tissue proximal to the fibrous regions of an infarct. As observed previously in Fig. 3, there is a marked decrease in the WT content as the proximity to an infarct increases, from 77% WT in the isolated distal cell to 39% WT in the isolated proximal cell (see Table S3). Relative to the distal subsection (Fig. 4C), the proximal subsection (Fig. 4D) presents 51.6% detection with the WT filter across the same area.

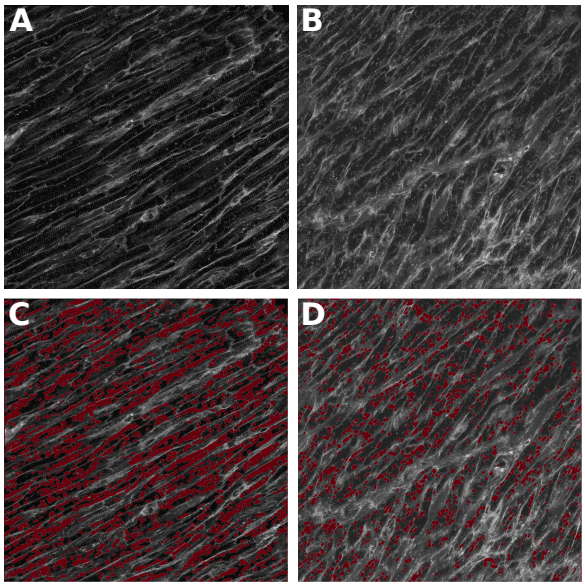

Figure 4: Application of algorithm to .3 mm^2 infarcted rabbit tissue subsections. A) and B) confocal data exhibiting conserved striations and a lack of observable striations, respectively. C) and D) algorithm output for confocal data using WT filter.

Limitations

While we believe the matched filtering approach provides a step forward toward classification of microscopy data, several limitations must be considered. Brute force application of the approach to large images can quickly become cost-prohibitive, as the memory required to process large images scales rapidly with size. Hence, where characterization of large tissue sections are needed, the image could be discretized into smaller sub-images,

or utilize intelligent downsampling techniques including wavelet analysis[33] or eigen-analysis[34] to reduce the information density. An additional limitation is that application of the algorithm to arbitrary data would require the user to tune the threshold parameters to optimize performance, given variations in immunofluorescence labeling, microscope performance and cell structure. In this study, we determined optimal parameters through ROC analysis, yet this approach still necessitated hand annotation to produce training data. In contrast, popular detection algorithms such as AUTOTT[27] have relatively few parameters requiring optimization and thus may be less difficult to apply to new data sets. Lastly, for filters that have considerable spectral information in common, it can be challenging to unambiguously discriminate between similar data features. In this study, we considered filters with strongly different features, e.g. the longitudinal features were orthogonal to the transverse, which reduced overlap. Nevertheless, we found that introducing a penalty parameter was necessary to improve detection performance (see Sect. S.1.4 for more details).

CONCLUSIONS

Our matched filtering-based technique complements existing computational algorithms for performing automated analysis of myocyte ultrastructure.[26,27] This approach leverages detailed structural information for the feature of interest, namely transverse tubules in this case. Its reliance on convolution permits local assessments of remodeling that may otherwise be difficult to achieve using techniques that are not designed with feature detection in mind. We found for the small bank of filter rotations and tubule morphologies tested that the approach performed remarkably well across diverse myocytes from different species and disease etiologies.

For the myocytes we considered, the approach revealed interesting trends in regional variation of myocyte ultrastructure, such as the heterogeneity of TT organization in SHAM cells, as well as intracellular remodeling severity that depended on the distance from a myocardial infarct. We anticipate that these variations may give important clues into how individual cells adapt to the contractile demands of their tissue environment or more generally, a specific phenotype. This topic was extensively explored by Guo et al,[10] wherein the authors cataloged diverse morphological configurations of myocyte ultrastructure with respect to species and disease etiology.

Correlations between TT disorganization and Ca^{2+} release dyssynchrony in numerous models of cardiac dysfunction[31,35–37] suggest strong linkages between myocyte morphology and pathophysiological function. Intriguingly, it has been observed that sarcolemmal proteins can redistribute under certain conditions that correlate with Ca^{2+} mismanagement, in the absence of TT loss.[37] Accordingly, it will be invaluable to investigate the potential correlations between TT remodeling and protein localization, as well as the extent to which those relationships influence normal physiological function. In this regard, although the data considered in this study was limited to confocal images of dye-labeled sarcolemma, it is fundamentally straightforward to adapt the algorithm to diverse data sets. Hence, in the event that filters representing features of interest can be identified, the approach can be adapted to a host of different labeling and imaging techniques, as well as cells isolated from a spectrum of cardiac tissue types.

Acknowledgements

Research reported in this publication, release was supported by the Maximizing Investigators' Research Award (MIRA) (R35) from the National Institute of General Medical Sciences (NIGMS) of the National Institutes of Health (NIH) under grant number R35GM124977, as well as an Institutional Development Award (IDeA) from the National Institute of General Medical Sciences (NIGMS) of the National Institutes of Health (NIH) under grant number P20GM103527. We would like to thank Mr. Noah Adler for his support in integrating our utilities onto a web platform, as well as Darin Vaughan for critical discussion of the manuscript.

References

[1] D. M. Bers. *Excitation-Contraction Coupling and Cardiac Contractile Force*. Ed. by D. M. Bers. Vol. 1. Kluwer Academic Publishers: Kluwer Academic Publishers, 2001, p. 427. ISBN: 9780792371588.

[2] S. E. Litwin, J. Li, and J. H. B. Bridge. "Na-Ca Exchange and the Trigger for Sarcoplasmic Reticulum Ca Release: Studies in Adult Rabbit Ventricular Myocytes". In: *Biophysical Journal* 75.1 (July 1998), pp. 359–371. ISSN: 0006-3495.

[3] M. Stern. "Theory of excitation-contraction coupling in cardiac muscle". In: *Biophysical Journal* 63.2 (Aug. 1992), pp. 497–517. ISSN: 0006-3495.

[4] X. H. Sun et al. "Molecular architecture of membranes involved in excitation-contraction coupling of cardiac muscle." In: *The Journal of cell biology* 129.3 (May 1995), pp. 659–71. ISSN: 0021-9525.

[5] C. Soeller et al. "Examination of the transverse tubular system in living cardiac rat myocytes by 2-photon microscopy and digital image-processing techniques." In: *Circulation research* 84.3 (Feb. 1999), pp. 266–75. ISSN: 0009-7330.

[6] J. Amsellem et al. "Transverse-axial tubular system in guinea pig ventricular cardiomyocyte: 3D reconstruction, quantification and its possible role in K+ accumulation-depletion phenomenon in single cells". In: *Biology of the Cell* 85.1 (Jan. 1995), pp. 43–54. ISSN: 0248-4900.

[7] D. M. Bers. "Altered cardiac myocyte Ca regulation in heart failure." In: *Physiology (Bethesda, Md.)* 21.17 (2006), pp. 380–387. ISSN: 1548-9213.

[8] W. E. Louch, O. M. Sejersted, and F. Swift. "There Goes the Neighborhood: Pathological Alterations in T-Tubule Morphology and Consequences for Cardiomyocyte Ca2+ Handling". In: *Journal of Biomedicine and Biotechnology* 2010 (2010), pp. 1–18.

[9] W. E. Louch et al. "T tubule disorganization and reduced synchrony of Ca2+ release in murine cardiomyocytes following myocardial infarction". In: *The Journal of Physiology* 574.2 (2006), pp. 519–533.

[10] A. Guo et al. "Emerging mechanisms of T-tubule remodelling in heart failure". In: *Cardiovascular Research* 98.2 (May 2013), pp. 204–215. ISSN: 0008-6363.

[11] T. O. Stølen et al. "Interval training normalizes cardiomyocyte function, diastolic Ca2+ control, and SR Ca2+ release synchronicity in a mouse model of diabetic cardiomyopathy." In: *Circulation Research* 105.6 (2009), pp. 527–536.

[12] F. Swift et al. "Extreme sarcoplasmic reticulum volume loss and compensatory T-tubule remodeling after Serca2 knockout". In: *Proceedings of the National Academy of Sciences* 109.10 (2012), pp. 3997–4001. ISSN: 0027-8424.

[13] L.-S. Song et al. "Calcium Biology of the Transverse Tubules in Heart". In: *Annals of the New York Academy of Sciences* 1047.1 (2006), pp. 99–111.

[14] C. Ferrantini et al. "Impact of detubulation on force and kinetics of cardiac muscle contraction." In: *The Journal of general physiology* 143.6 (2014), pp. 783–97. ISSN: 1540-7748.

[15] L. Øyehaug et al. "Synchrony of Cardiomyocyte Ca2+ Release is Controlled by t-tubule Organization, SR Ca2+ Content, and Ryanodine Receptor Ca2+ Sensitivity". In: *Biophysical Journal* 104.8 (Apr. 2013), pp. 1685–1697. ISSN: 00063495.

[16] L. Li et al. "Calcium Dynamics in the Ventricular Myocytes of SERCA2 Knockout Mice: A Modeling Study". In: *Biophysical Journal* 100.2 (2011), pp. 322–331.

[17] W. E. Louch et al. "Slow Ca2+ sparks de-synchronize Ca2+ release in failing cardiomyocytes: Evidence for altered configuration of Ca2+ release units?" In: *Journal of molecular and cellular cardiology* 58 (2013), pp. 41–52.

[18] P. M. Kekenes-Huskey et al. "Modeling effects of L-type ca(2+) current and na(+)-ca(2+) exchanger on ca(2+) trigger flux in rabbit myocytes with realistic T-tubule geometries." In: *Frontiers in physiology* 3 (2012), p. 351. ISSN: 1664-042X. arXiv: PMC3463892.

[19] E. Savio-Galimberti et al. "Novel features of the rabbit transverse tubular system revealed by quantitative analysis of three-dimensional reconstructions from confocal images". In: *Biophysical Journal* 95.4 (2008), pp. 2053–2062.

[20] N. S. Torres et al. "A modified local control model for Ca2+ transients in cardiomyocytes: junctional flux is accompanied by release from adjacent non-junctional RyRs." In: *Journal of molecular and cellular cardiology* 68 (2014), pp. 1–11.

[21] H. Li et al. "Cardiac Resynchronization Therapy Reduces Subcellular Heterogeneity of Ryanodine Receptors, T-Tubules, and Ca2+ Sparks Produced by Dyssynchronous Heart Failure". In: *Circulation: Heart Failure* 8.6 (2015), pp. 1105–1114. ISSN: 19413297.

[22] F. B. Sachse et al. “Subcellular Structures and Function of Myocytes Impaired During Heart Failure Are Restored by Cardiac Resynchronization Therapy”. In: *Circulation Research* 110.4 (2012), 588–U197.

[23] D. J. Crossman et al. “Changes in the organization of excitation-contraction coupling structures in failing human heart”. In: *PLoS ONE* 6.3 (2011), e17901.

[24] A. R. A. R. Lyon et al. “Loss of T-tubules and other changes to surface topography in ventricular myocytes from failing human and rat heart.” In: *Audio, Transactions of the IRE Professional Group on* 106.16 (2009), pp. 6854–6859.

[25] K.-L. Ang et al. “Limitations of conventional approaches to identify myocyte nuclei in histologic sections of the heart”. In: *American Journal of Physiology - Cell Physiology* 298.6 (2010).

[26] C. Pasqualin et al. “Automatic quantitative analysis of t-tubule organization in cardiac myocytes using ImageJ”. In: *American Journal of Physiology - Cell Physiology* 308.3 (2015), pp. C237–C245.

[27] A. Guo and L.-S. Song. “AutoTT: automated detection and analysis of T-tubule architecture in cardiomyocytes.” In: *Biophysical journal* 106.12 (June 2014), pp. 2729–36. ISSN: 1542-0086.

[28] R. Arora et al. “Regional distribution of T-tubule density in left and right atria in dogs”. In: *Heart Rhythm* 14.2 (2017), pp. 273–281.

[29] S. M. Pizer et al. “Adaptive histogram equalization and its variations”. In: *Computer Vision, Graphics, and Image Processing* 39.3 (Sept. 1987), pp. 355–368. ISSN: 0734-189X.

[30] H. L. Van Trees. *Detection, Estimation, and Modulation Theory, Part I.* New York, USA: John Wiley & Sons, Inc., Sept. 2001, p. 716. ISBN: 0471095176.

[31] W. E. Louch et al. “T-tubule disorganization and reduced synchrony of Ca ¡sup¿2+¡/sup¿ release in murine cardiomyocytes following myocardial infarction”. In: *The Journal of Physiology* 574.2 (July 2006), pp. 519–533. ISSN: 00223751.

[32] M. Frisk et al. “Elevated ventricular wall stress disrupts cardiomyocyte t-tubule structure and calcium homeostasis”. In: *Cardiovascular Research* 112.1 (Oct. 2016), pp. 443–451. ISSN: 0008-6363.

[33] G. Strang and T. Nguyen. *Wavelets and Filter Banks.* 1st ed. Wellesley-Cambridge Press, 1996. ISBN: 9780961408879.

[34] M. Turk and A. Pentland. “Eigenfaces for Recognition”. In: *Journal of Cognitive Neuroscience* 3.1 (Jan. 1991), pp. 71–86. ISSN: 0898-929X.

[35] H. K. Mørk et al. “Slowing of cardiomyocyte Ca ¡sup¿2+¡/sup¿ release and contraction during heart failure progression in postinfarction mice”. In: *American Journal of Physiology-Heart and Circulatory Physiology* 296.4 (Apr. 2009), H1069–H1079. ISSN: 0363-6135.

[36] I. Lenaerts et al. “Ultrastructural and Functional Remodeling of the Coupling Between Ca2+ Influx and Sarcoplasmic Reticulum Ca2+ Release in Right Atrial Myocytes From Experimental Persistent Atrial Fibrillation”. In: *Circulation Research* 105.9 (Oct. 2009), pp. 876–885. ISSN: 0009-7330.

[37] F. Swift et al. “Extreme sarcoplasmic reticulum volume loss and compensatory T-tubule remodeling after Serca2 knockout”. In: *Proceedings of the National Academy of Sciences* 109.10 (Mar. 2012), pp. 3997–4001. ISSN: 0027-8424.

[38] F. B. Sachse et al. “Sub-micrometer anatomical models of the sarcolemma of cardiac myocytes based on confocal imaging”. In: *Pacific Symposium on Biocomputing 2008: Kohala Coast, Hawaii, USA, 4-8 January 2008* (2008), p. 390.

[39] T. Hayashi et al. “Three-dimensional electron microscopy reveals new details of membrane systems for Ca2+ signaling in the heart.” In: *Journal of Cell Science* 122.Pt 7 (Apr. 2009), pp. 1005–13.

[40] J. Wong et al. “Nanoscale Distribution of Ryanodine Receptors and Caveolin-3 in Mouse Ventricular Myocytes: Dilation of T-Tubules near Junctions”. In: *Biophysical Journal* 104.11 (2013), pp. L22–L24.

[41] T. Seidel et al. “Sheet-Like Remodeling of the Transverse Tubular System in Human Heart Failure Impairs Excitation-Contraction Coupling and Functional Recovery by Mechanical Unloading”. In: *Circulation* 135.17 (2017), pp. 1632–45.

[42] T. Seidel, A. Sankarankutty, and F. Sachse. “Remodeling of the transverse tubular system after myocardial infarction in rabbit correlates with local fibrosis: A potential role of biomechanics”. In: *Progress in Biophysics and Molecular Biology* (July 2017). ISSN: 00796107.

[43] B. Efron and R. Tibshirani. *An Introduction to the Bootstrap.* 1st ed. Chapman & Hall/CRC Monographs on Statistics & Applied Probability (Book 57), 1993, p. 456. ISBN: 9780412042317.

[44] P. Jouannot and P. Hatt. “Rat myocardial mechanics during pressure-induced hypertrophy development and reversal”. In: *American Journal of Physiology-Legacy Content* 229.2 (Aug. 1975), pp. 355–364.

[45] S. Wei et al. "T-tubule remodeling during transition from hypertrophy to heart failure." In: *Circulation research* 107.4 (Aug. 2010), pp. 520–31.

[46] A. R. Lyon et al. "Loss of T-tubules and other changes to surface topography in ventricular myocytes from failing human and rat heart." In: *Proceedings of the National Academy of Sciences of the United States of America* 106.16 (Apr. 2009), pp. 6854–9. ISSN: 1091-6490.